

Andreev spectroscopy of doped HgTe quantum wells

M. Guigou and J. Cayssol
*CPMOH, UMR 5798, Université Bordeaux I,
 33405 Talence, France*

We investigate the Andreev reflection process in high-mobility HgTe/CdTe quantum wells. We find that Andreev conductance probes the dynamics of massive 2+1 Dirac fermions, and that both specular Andreev reflection and retroreflection can be realized even in presence of a large mismatch between the Fermi wavelengths at the two sides of the normal/superconducting junction.

I. INTRODUCTION

Three dimensional topological insulators (TIs) and two dimensional Quantum Spin Hall (QSH) states are novel electronic phases which are characterized by topological invariants rather than by spontaneously broken symmetries¹⁻³. Both QSH states and TIs are distinguished from ordinary insulators by the presence of conducting edge or surface states surrounding an insulating bulk⁴⁻⁷. These protected boundary states were experimentally confirmed in HgTe quantum wells^{8,9}, and in three dimensional TIs like Bi_{1-x}Sb_x¹⁰, Bi₂Te₃ and Bi₂Se₃^{11,12}.

All these materials follow a general mechanism whereby the strong spin-orbit interaction drives an inversion between bands of distinct symmetry⁵, e.g. opposite parities⁶. Simple massive Dirac equations describe altogether the conduction/valence and the spin degrees of freedom of QSH systems or TIs, the crucial band inversion feature being captured by the sign of the mass term^{1-3,5}. Therefore doped HgTe quantum wells are also model systems to investigate the dynamics of massive Dirac fermions in 2+1 dimensions¹⁴⁻¹⁶.

Combining these unique topological phases with conventional superconductivity raises fundamental questions about topological superconductors^{17,18}, and may lead to the discovery of novel exotic modes such as Majorana fermions¹⁹⁻²⁴ with potential applications for spintronics and quantum computing²⁵. Previously most studies have focused on proximity induced superconductivity within 1D edge states^{20,26} or 2D surface states^{19,21-23}. In doped TIs (resp. QSH systems), the fluctuations should be less detrimental to superconductivity than in the 2D (or 1D) boundary states available in the insulating regime. Indeed superconductivity was recently reported in the topological insulator Bi₂Se₃ doped with copper atoms²⁷ while Heusler superconductors²⁸ or Thallium based chalcogenides²⁹ are promising candidates for a topological superconductor.

In this context it is of primary importance to understand proximity effect between a doped topological insulator and a s-wave singlet superconductor. The fundamental scattering process is the Andreev reflection (AR) whereby an incident electron is converted into a reflected hole at the interface between a normal metal and a superconductor^{30,31}. Moreover it was recently predicted that relativistic electrons in graphene may experience an

unusual specular Andreev reflection³²⁻³⁴.

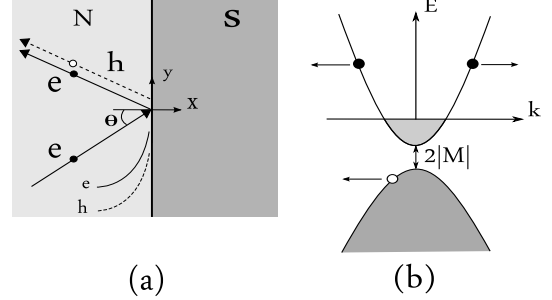


FIG. 1: (a) Normal/superconductor (NS) contact. (b) Schematic band structure where $2|M|$ is the bulk gap and M the mass. The black dots represent the incident and reflected electrons while the open dot stands for the Andreev reflected hole (here interband specular reflection is shown). Arrows represent group velocities.

In this paper, we show that AR can be used as a probe of the carrier dynamics in HgTe quantum wells which is intermediate between linear and quadratic dispersion. As low gap semiconductors, HgTe wells also exhibit a specular Andreev reflection which is sensitive to band inversion. While we use HgTe for calculations, the general features are expected to apply for other two-dimensional QSH systems³⁵ and for three dimensional TIs^{7,11,12}. Our findings also complete previous studies of the Andreev conductance of a NS contact in presence of Rashba spin orbital coupling³⁶.

The paper is organized as follows. In Sec II we introduce the model for the NS contact. The energy and angular dependences of the Andreev reflection processes are described in Sec. III. These single channel results are used in Sec IV to obtain the multichannel differential conductance which is the relevant quantity for transport experiments.

II. MODEL

In this section, we present the model of the NS junction and describe the scattering formalism used to compute the Andreev probability and the differential conductance.

A. Hamiltonian

We consider a thin HgTe quantum well realized between two identical CdTe barriers. The two-dimensional subbands of such quantum wells have been derived from the Kane model of HgTe and CdTe using the envelope function method³⁷. The QSH state is related to the crossing between the electron-like subband $E1$ and the heavy hole-like subband $H1$ which is controlled by the HgTe layer width⁵. When the bulk inversion asymmetry is neglected, those relevant bands are degenerated with respect to the spin index (\pm) and have opposite parity eigenvalues. Then the low energy dynamics of this four-band model is captured by the massive Dirac Hamiltonian⁵

$$H(\mathbf{k}) = \begin{pmatrix} h(\mathbf{k}) & 0 \\ 0 & h^*(-\mathbf{k}) \end{pmatrix}, \quad (1)$$

given in the basis order ($|E1+\rangle, |H1+\rangle, |E1-\rangle, |H1-\rangle$). The spin up block $h(\mathbf{k}) = \varepsilon(\mathbf{k}) + d_a(\mathbf{k})\sigma_a$ is expressed in terms of the standard Pauli matrices σ_a ($a = 1, 2, 3$) acting in ($|E1\rangle, |H1\rangle$) space. The Hamiltonian $H(\mathbf{k})$ is a Taylor expansion with respect to the in-plane wavevector $\mathbf{k} = (k_x, k_y)$ whose coefficients are constrained by parity and time-reversal symmetries. Microscopic theory further yields that $d_a = (Ak_x, -Ak_y, M(k) = M - Bk^2)$ and $\varepsilon(\mathbf{k}) = C - Dk^2$, where $k^2 = k_x^2 + k_y^2$. The parameters A, B, C, D and M depend on the quantum well geometry⁵. In particular, the inversion between $|E1\rangle$ and $|H1\rangle$ is controlled by the sign of the mass term M , the QSH state being realized in the inverted regime ($M < 0$). The chemical potential C determines the electronic filling of the bands which can be electrostatically tuned by the action of a distant metallic gate.

We assume that a singlet s-wave superconductor induces a pairing potential in some region of a ballistic HgTe/CdTe quantum well. Thereby the Hamiltonian of Eq.(1) must be completed by particle-hole (or charge conjugation) symmetry leading in principle to an eight by eight Bogoliubov-de Gennes Hamiltonian. Since superconductivity only pairs time-reversed states, a spin up electron will be coupled with a hole in the spin down band. Therefore electrons and holes are described by two decoupled (four by four) Bogoliubov-de Gennes-Dirac equations like

$$\begin{pmatrix} h(-i\hbar\partial_{\mathbf{r}}) & \Delta(\mathbf{r}) \\ \Delta^*(\mathbf{r}) & -h(-i\hbar\partial_{\mathbf{r}}) \end{pmatrix} \Psi(\mathbf{r}) = E\Psi(\mathbf{r}), \quad (2)$$

where $\Psi(\mathbf{r}) = (\Psi_{E1+}, \Psi_{H1+}, \Psi_{E1-}^*, \Psi_{H1-}^*)$, and the absence of magnetic field is assumed. The excitation energy E is measured from the Fermi level. The matrix Δ is diagonal at the lowest order approximation in momentum. In principle the diagonal entries, Δ_E and Δ_H , of the pairing matrix are not equal because $|E1\rangle$ and $|H1\rangle$ involve different combinations of atomic orbitals. Nevertheless we first assume that $\Delta_E = \Delta_H = \Delta_0 e^{i\phi}$ for simplicity. In a uniform system, the eigenmodes of Eq.(2) are plane

waves with momentum \mathbf{k} and energy

$$E(\mathbf{k}) = \sqrt{(\varepsilon(\mathbf{k}) \pm d(\mathbf{k}))^2 + \Delta_0^2}, \quad (3)$$

with $d(\mathbf{k}) = \sqrt{A^2 k^2 + (M - Bk^2)^2}$. The \pm sign refers to the conduction/valence subbands.

B. Scattering problem

We now consider a straight normal/superconducting interface at $x = 0$ (Fig.1). The normal side ($x < 0$) is described by Eq.(2) with $C(\mathbf{r}) = C_N$ and $\Delta(\mathbf{r}) = 0$, while the superconducting side may have a distinct electronic filling fixed by $C(\mathbf{r}) = C_S$ and a uniform pairing potential $\Delta(\mathbf{r}) = \Delta_0 e^{i\phi}$. This sharp step model is valid when the potentials vary on typical scales smaller than the Fermi wavelength of the carriers in HgTe. We further assume a perfect interface which is relevant for high quality contacts. Previously a NS contact in the presence of Rashba spin-orbit coupling was already considered in the context of spintronics³⁶. The main distinction between the HgTe/CdTe effective Hamiltonian and similar Rashba systems consists in the presence the $(m - Bk^2)\sigma_3$ term in Eqs. (1,2).

We solve the scattering problem with an incoming spin up quasiparticle in the conduction band. Since the scattering is elastic and the problem invariant by translation along y -axis, the excitation energy E and the transverse momentum k_y are conserved. Hence all the scattered waves are written hereafter as $\Psi(x)e^{ik_y y}$.

In the normal part, $x < 0$, electrons and holes are decoupled since $\Delta(\mathbf{r}) = 0$. The electron-like quasiparticles are described by four-spinor plane-waves

$$\Psi_e(x) = \begin{pmatrix} T \\ \chi_{\pm}(\mathbf{k}_e), 0, 0 \end{pmatrix} e^{ik_{ex}x}, \quad (4)$$

with $\chi_{\pm}(\mathbf{k}) = (\pm d(\mathbf{k}) + M(\mathbf{k}), A(k_x - ik_y))^{14-16}$. The upperscript T denotes transpose and the \pm sign corresponds to the conduction or the valence subband. For a n -doped HgTe well, the Fermi level lies in the conduction subband. The dispersion equation, $C_N - Dk^2 + d(\mathbf{k}) = E$, allows for two possible values of k^2 :

$$k_{1,2}^2(E) = \frac{1}{2(B^2 - D^2)} \left[\gamma \pm \sqrt{\gamma^2 - 4(B^2 - D^2)(M^2 - (C_N - E)^2)} \right], \quad (5)$$

where $\gamma = -A^2 + 2MB - 2(C_N - E)D$ and $B^2 > D^2$. The positive one, ($k_1^2 > 0$), corresponds to a the propagative mode in the bulk, while an additional evanescent mode ($k_2^2 < 0$) shows up at interfaces¹³⁻¹⁶. The incident and reflected electrons have longitudinal momentum $k_{ex} = k_1 \cos \theta$, and $-k_1 \cos \theta$ respectively, θ being the incidence angle (Fig.1). The evanescent electron is described by a complex momentum $k_{ex} = -i(-k_2^2 + k_y^2)^{1/2}$.

The hole-like quasiparticles are also described by the four-spinor plane-waves

$$\Psi_h(x) = \begin{pmatrix} T \\ 0, 0, \chi_{\pm}(\mathbf{k}_h) \end{pmatrix} e^{ik_{hx}x}. \quad (6)$$

The longitudinal wavevectors k_{hx} is obtained by solving the equation $C_N - Dk^2 + d(\mathbf{k}) = -E$ for a hole in the conduction band (intraband AR) or $C_N - Dk^2 - d(\mathbf{k}) = -E$ for a hole in the valence band (interband AR).

In the superconducting part ($x > 0$), the eigenmodes are four Bogoliubov quasiparticles which are all evanescent below the gap ($E < \Delta_0$)

$$\Psi_{S\pm}(x) = \begin{pmatrix} T \\ \chi_{\pm}(\mathbf{k}_S), \chi_{\pm}(\mathbf{k}_S) e^{\pm i\beta} \end{pmatrix} e^{\pm i k_{Sx} - \kappa} x, \quad (7)$$

$$\Psi'_{S\pm}(x) = \begin{pmatrix} T \\ \chi_{\pm}(\mathbf{k}'_S), \chi_{\pm}(\mathbf{k}'_S) e^{\pm i\beta} \end{pmatrix} e^{\pm i k'_{Sx} \pm i\kappa} x, \quad (8)$$

where $\kappa = \sqrt{\Delta_0^2 - E^2}/\hbar v_F$ is an inverse coherence length. The phase $\beta = \arccos(E/\Delta_0)$ is intrinsically related to electron-hole conversion at a normal conductor-superconductor interface³⁰. We have introduced the wavevectors $k_{Sx} = (k_{1S}^2 - k_y^2)^{1/2}$ and $k'_{Sx} = i(k_y^2 - k_{2S}^2)^{1/2}$, where k_{1S}^2 and k_{2S}^2 are defined by Eq.(5) under the substitution $C_N \rightarrow C_S$ and $E = 0$. The scattering amplitudes of the four reflected modes and four evanescent transmitted modes in the superconductor are determined by writing the continuity of the wavefunction and of its derivative at $x = 0$ (Appendix A).

C. Andreev differential conductance

When a positive bias V is applied to the normal side with respect to the superconductor, the current I is carried by the injected electrons, the reflected electrons (with amplitude $r_{ee}(E, \theta)$) and the Andreev reflected holes (with amplitude $r_{he}(E, \theta)$). The corresponding differential conductance of the NS interface can be written³¹

$$\frac{\partial I}{\partial V} = g_0(eV) \int dE \left(-\frac{\partial f}{\partial E} \right) \int_{-\frac{\pi}{2}}^{\frac{\pi}{2}} d\theta \cos\theta (1 - R(E, \theta) + R_A(E, \theta)), \quad (9)$$

where $g_0(eV) = e^2 k_1(eV)W/(\pi\hbar)$, W is the width of the HgTe quantum well along y -axis and $f = f(E - eV) = 1/(e^{(E-eV)/T} + 1)$ is the Fermi distribution of incident electrons in the normal lead N at temperature T . The probability for an electron of energy E to be reflected as an electron is $R(E, \theta) = |r_{ee}(E, \theta)|^2$ while $R_A(E, \theta) = \frac{j(E, \theta)}{j(-E, \theta)} |r_{he}(E, \theta)|^2$ denotes the probability for Andreev reflection as a hole. The average current

$$j(E, \theta) = -2k_1(E) \cos\theta \{ (D+B)(d(\mathbf{k}) + M(\mathbf{k}))^2 + A^2 k^2 (D-B) - A^2 (d(\mathbf{k}) + M(\mathbf{k})) \}, \quad (10)$$

is derived by the standard quantum mechanical procedure (Appendix B).

III. SINGLE CHANNEL ANDREEV REFLECTION

In this section, we investigate the Andreev reflection process for a single channel which is labelled by its energy E and incidence angle θ . We contrast the behaviors of the Andreev reflection probability $R_A(E, \theta)$ at high and low doping levels in the normal part of the NS junction. In the later case, the subgap Andreev reflection can be either an intraband or interband process whereas it is always intraband in heavy doped wells. In both cases, varying the ratio B/A allows to turn continuously the Andreev reflection probability $R_A(E, \theta)$ from the one obtained in graphene/superconductor junctions to the one for standard metal/superconductor junctions.

A. Heavy doping $|C_N| \gg \Delta_0$

We first consider HgTe wells with typical metallic doping, *i.e.* $|C_N| \gg \Delta_0$. Then an incident electron (energy E) from the conduction band always finds an electron of the same band (energy $-E$) to form a Cooper pair thereby realizing an intraband Andreev conversion. Therefore the Andreev reflection is a standard retroreflection because the electron energy E is always much smaller than the conduction band Fermi energy $|C_N|$.

We find that the probability $R_A(E, \theta = 0)$ is strictly monotonic (increasing) below the gap, and presents a singularity at $eV = \Delta_0$. The AR probability is controlled by the Fermi wavelength mismatch (FWM) between the normal and superconducting sides, and usually decreases when the FWM increases. At given electronic fillings (or FWM), the Andreev probability is suppressed when the ratio B/A is increased, namely when going from Dirac (purely linear dispersion) to Schrödinger (purely quadratic dispersion) dynamics (Fig. 2). This crossover is characterized by the dimensionless parameter $\lambda = k_1(0)B/A = (n/n_0)^{1/2}$, where $n = k_1^2(0)/(2\pi)$ is the two-dimensional carrier density in the conduction subband while $n_0 = A^2/(2\pi B^2) \simeq 5.10^{12} \text{ cm}^{-2}$ for $A = 4 \text{ eV} \cdot \text{\AA}$ and $B = -70 \text{ eV} \cdot \text{\AA}^2$. When electrons are injected through the junction with a finite incidence angle, the Andreev reflection probability decreases but has qualitatively the same energy dependence than the $\theta = 0$ mode (Fig. 2). The general crossover between purely linear or quadratic dispersion still pertains for any incidence angle.

B. Low doping $|C_N| < \Delta_0$

We now turn to the case of low doping in the normal side, namely $|C_N| < \Delta_0$. At low voltage bias ($0 < eV < |C_N| - |M|$), the reflected hole belongs to conduction band thereby realizing the standard intraband AR which is a retroreflection. At intermediate

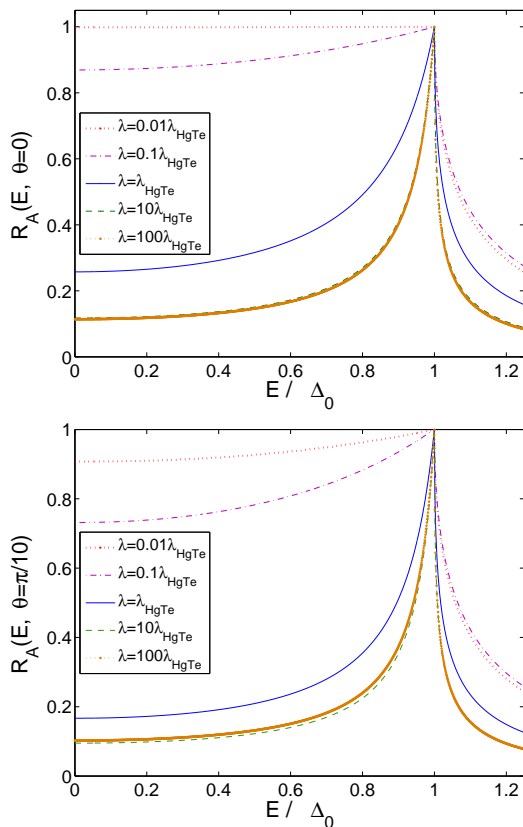


FIG. 2: (Color Online). Single channel Andreev reflection probability through the NS junction for $\theta = 0$ (top panel) and $\theta = \pi/10$ (bottom panel). The electronic fillings are set by $-C_N = 30$ meV and $-C_S = 1$ eV, while the induced gap is $\Delta_0 = 1$ meV. All curves are plotted for $A = 4$ eV $\cdot\text{\AA}$, and in the inverted regime $M = -0.1\Delta_0$. The Andreev reflection probability is progressively suppressed when the quadratic dispersion is increased: $-B = 0.7; 7; 70; 700$ and 7000 eV $\cdot\text{\AA}^2$ from top to bottom. In contrast to B , the parameter D has very little impact on Andreev reflection probability provided $|B| > |D|$. Hence we have set $D = 0$ in order to allow for a broader window of variation for the parameter B .

voltages ($|C_N| - |M| < eV < |C_N| + |M|$), the AR is completely suppressed in the bulk because the hole should be in the semiconducting gap. At higher voltages ($eV > |C_N| + |M|$), the reflected hole corresponds to the removal of a valence band electron. Then the AR is an interband process and a specular reflection. In brief, Andreev reflection allows for a spectroscopy of the HgTe/CdTe well 2D spectrum since for instance the energy window where the AR is totally suppressed is $2|M|$, i.e. twice the semiconducting gap, for the mode $\theta = 0$.

Moreover at the bottom of the conduction band, a singularity appears in the AR probability at $E = |C_N| - |M|$ and normal incidence (blue solid curve in Fig. 3). Nevertheless, this abrupt behavior becomes smoother when electrons are injected with a non zero angle and the AR probability decreases.

Furthermore the energy window where the Andreev

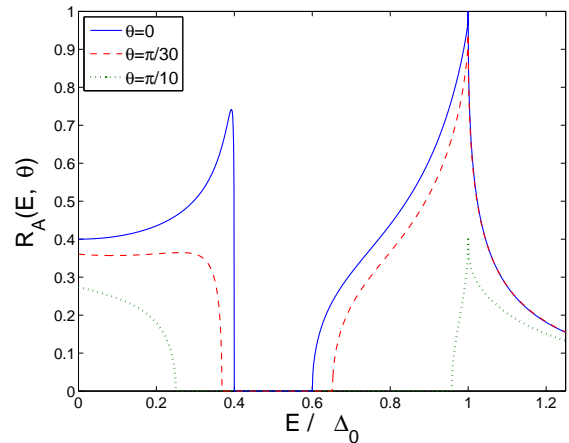


FIG. 3: (Color Online). Single channel Andreev reflection probability in the inverted regime ($M = -0.1\Delta_0$) at low doping ($-C_N = 0.5\Delta_0$) and for three different incidence angles: $\theta = 0$ (blue solid line), $\theta = \pi/30$ (red dashed line) and $\theta = \pi/10$ (green dotted line). The other parameters are taken from typical HgTe wells: $A = 4$ eV $\cdot\text{\AA}$, $B = -70$ eV $\cdot\text{\AA}^2$, $D = -50$ eV $\cdot\text{\AA}^2$. The superconductor is heavily doped (Fermi energy $-C_S = 1$ eV).

reflection is totally suppressed ($R_A(E, \theta) = 0$) broadens while increasing incidence angle (Fig. 3). This phenomenon has the following explanation. Owing to translational invariance along the NS interface, the transverse momentum k_y is conserved and one has to solve an effective one-dimensional scattering problem for each value of k_y . It turns out that a finite k_y acts as a supplementary mass/gap in this 1D scattering problem. For instance, when $M = 0$ the 2D system is gapless but the 1D problem (described by the dispersion relation $E(k_x, k_y)$ for defined k_y) acquires a gap proportionnal to the transverse momentum, as it is well known in graphene³⁸.

IV. DIFFERENTIAL CONDUCTANCE

In this section, we focus on the differential $\partial I/\partial V$ conductance of the NS contact which is obtained by angular integration over all the transverse channels. The $\partial I/\partial V$ characteristics are qualitatively distinct in the low and in the heavily doped regimes respectively, and they depend quantitatively upon the ratio B/A and the Fermi wavelength mismatch (FWM).

A. Heavy doping $|C_N| \gg \Delta_0$

The voltage dependance of the differential conductance $\partial I/\partial V$ is inherited from the energy dependence of the AR probability through Eq.(9). Hence, in the case of heavy doping in the N region, the $\partial I/\partial V$ characteristics are also strictly increasing below the gap, and present a singularity at $eV = \Delta_0$ (compare Fig. 4 and Fig. 2).

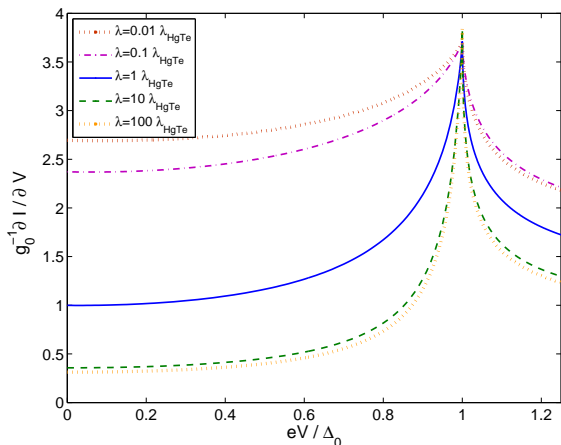


FIG. 4: (Color online). Differential conductance of NS contact normalised by $g_0(eV) = e^2 k_1(eV)W / (\pi h)$. Both side of the junction are heavily doped $-C_N = 30$ meV and $-C_S = 1$ eV. All curves are plotted for $A = 4$ eV \cdot \AA , and in the inverted regime $M = -0.1\Delta_0$. The Andreev conductance is plotted for different values of B : $-B = 0.7; 7; 70; 700$ and 7000 eV \cdot \AA^2 from top to bottom. As in Figs. 2, the red dotted curve is identical to the graphene case up to a factor 2 due to the absence of valley degeneracy in HgTe and the blue solid curve corresponds to typical parameters for current HgTe/CdTe. We have set $D = 0$.

The differential conductance of a normal potential step is asymptotically recovered far above the gap ($eV \gg \Delta_0$).

We now discuss the crossover between Dirac (purely linear dispersion) and Schrödinger (purely quadratic dispersion) dynamics (Fig. 4). For this purpose we use again the dimensionless parameter $\lambda = k_1(0)B/A$ defined in section III.A. The increase of the ratio B/A leads to the decay of the Andreev conductance. This result is in accordance with the fact that FWM strongly suppresses AR in standard metals³¹, whereas AR is very robust against FWM at a graphene/superconductor interface^{32,33}. These contrasted behaviors can be used to probe the relative strength of linear and quadratic dispersion in HgTe wells (Fig. 4).

Finally thin films of 3D TIs are ideal systems to probe the complete crossover regime since their effective parameters A and B can be tuned by varying the film thickness³⁵, whereas only M can be significantly varied in HgTe quantum wells.

B. Low doping $|C_N| < \Delta_0$

In the case of low doping in the normal side ($|C_N| < \Delta_0$), the subgap differential conductance reveals both the semiconducting gap and the sign of the mass M (Fig. 5). Foremost the behavior of the differential conductance shows the presence of the reflected hole in the conduction/valence band through the electron-hole conversion at the interface. As a function of the voltage bias, the AR process is successively an intraband pro-

cess ($0 < eV < |C_N| - |M|$), forbidden in the bulk ($(|C_N| - |M| < eV < |C_N| + |M|)$) and an interband process ($eV > |C_N| + |M|$) which is reminiscent of specular AR in graphene^{32,33}. Unfortunately the observation of specular AR in graphene was hindered so far by disorder effects occurring at low doping. We expect that specular AR should be more easily observed in HgTe quantum wells since actual samples are characterized by larger elastic mean free paths than in graphene on a substrate.

Unlike the Andreev reflection probability, the behavior of the differential conductance in the inverted regime does not emphasize any peak at energy corresponding to the bottom of the conduction band. At such energy, only one channel participates to the Andreev conductance so that its contribution is tiny compared to the number of channels that are considered in the ballistic conductance $g_0(E)$.

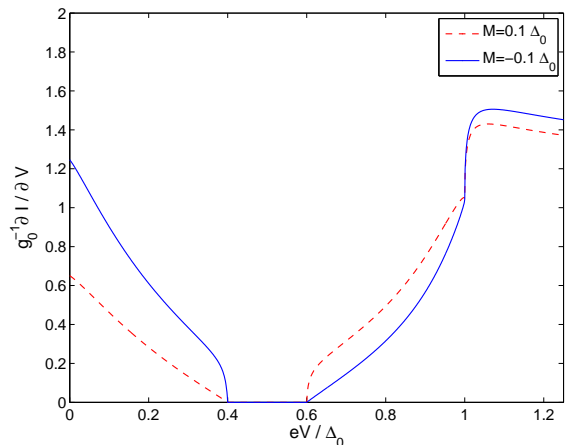


FIG. 5: (Color online). Differential conductance in the non inverted ($M = 0.1\Delta_0$, dashed red line) and inverted ($M = -0.1\Delta_0$, solid blue line) regime with $-C_N = 0.5\Delta_0$. The parameters A , B and D are the same than in Fig. 3.

Moreover there is a sizeable difference between the normal ($M/B < 0$) and the inverted regimes ($M/B > 0$) (Fig. 5). Below the gap, the interband specular AR is enhanced in the non inverted regime with respect to the inverted regime, whereas Andreev conduction is stronger in the inverted regime when $0 < eV < |C_N| - |M|$ (intraband AR) or above the gap. It should be emphasized that, even at the band crossing $M = 0$, the AR in HgTe/CdTe quantum wells differ from graphene owing to the presence of quadratic terms Bk^2 and Dk^2 in the Hamiltonian Eq.(2).

C. Experimental realization

The predicted differential conductance can be checked experimentally by realizing transparent enough contacts on existing mercury telluride heterostructures. In particular at low doping, the specular (interband) Andreev reflection could be observed in HgTe/CdTe quantum wells

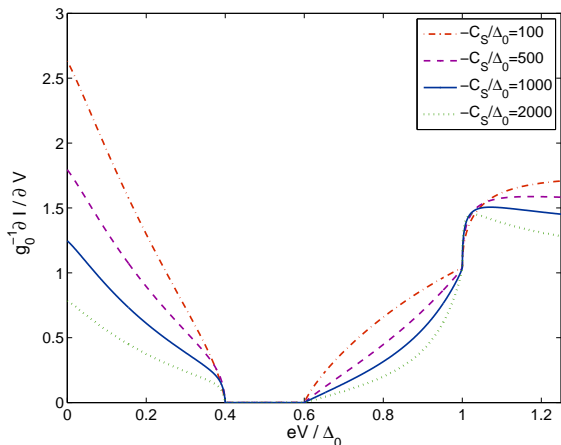


FIG. 6: (Color online). Influence of the Fermi energy $-C_S$ in the superconductor while $-C_N = 0.5\Delta_0$, $M = -0.1\Delta_0$. The values of the parameters A , B and D are the same than in Fig. 3.

with a superconducting contact. Nevertheless mass fluctuations, related to spatial variations of the HgTe layer width, may hinder the observation of specular AR in such low doped HgTe/CdTe wells (Fig. 5).

Another difficulty is related to the fact that the influence of doping in the superconducting region might be difficult to separate from the one of other parameters, like the mass M or the ratio B/A , using Andreev measurements only (Fig. 6). Moreover $|C_S|$ is neither controlled nor even known in contrast to $|C_N|$ which can be tuned by gating. We anticipate that future experiments will solve this issue by combining transport measurements through NN and NS junctions.

Finally, one should also expect in the inverted regime a contribution from the helical edge states. Since there is perfect Andreev reflection at a QSH insulator/superconductor junction, this contribution should be $4e^2/h$ ($2e^2/h$ per edge)²⁶. In the metallic regime, the large number of channels makes this edge conductance negligible with respect to the bulk conductance. Nevertheless near the band edges, i.e. at very low doping, the edge contribution becomes comparable with the bulk one.

V. CONCLUSION

In conclusion, Andreev conduction is a probe of the carrier dynamics in doped HgTe/CdTe quantum wells. Indeed the underlying AR mechanism is extremely sensitive to the balance between Schrödinger (purely quadratic dispersion) and Dirac (purely linear dispersion) dynamics. The unavoidable FWM between the normal and superconducting sides is not so harmful in HgTe/CdTe wells than in usual metals (but also more detrimental than in graphene). Furthermore we expect that our analysis of intraband AR pertains for

strong TIs in the doped regime, like Bi₂Se₃ or Bi₂Te₃, since they are described by similar effective Hamiltonians than HgTe/CdTe quantum wells^{1,7}. Nevertheless those large gap 3D TIs are less favorable than the small gap HgTe/CdTe wells for the observation of specular AR.

We thank Bjoern Trauzettel and Patrik Recher for very useful discussions. We acknowledge funding from the Agence Nationale de la Recherche under Grants No. ANR-07-NANO-011-05 (ELEC-EPR) and ANR-10-BLAN-xxx-xx (IsoTop). J.C. also acknowledges supports from the Institut de Physique Fondamentale de Bordeaux.

VI. APPENDIX

A. Boundary conditions

We provide a derivation of the boundary conditions we used in this paper to determine the scattering amplitudes.

The Bogoliubov-de Gennes matrix equation Eq.(2) consists in four scalar equations. For definiteness let us consider the first scalar equation:

$$(C + M)\Psi_{E1+}(x, y) + (D + B)(\partial_x^2 + \partial_y^2)\Psi_{E1+}(x, y) - iA\partial_x\Psi_{H1+}(x, y) + A\partial_y\Psi_{H1+}(x, y) + \Theta(x)\Delta_0 e^{i\phi}\Psi_{E1-}^*(x, y) = E\Psi_{E1+}(x, y), \quad (11)$$

where the Heaviside function $\Theta(x)$ indicates the presence of superconductivity only on the right side of the junction and where we made the substitution $k_{x,y} \rightarrow -i\partial_{x,y}$. Integrating Eq.(11) over the small region $[-\epsilon; \epsilon]$ around the interface, we obtain

$$(C + M) \int_{-\epsilon}^{\epsilon} dx \Psi_{E1+}(x, y) + (D + B) \int_{-\epsilon}^{\epsilon} dx (\partial_x^2 + \partial_y^2) \Psi_{E1+}(x, y) - iA \int_{-\epsilon}^{\epsilon} dx \partial_x \Psi_{H1+}(x, y) + A \partial_y \int_{-\epsilon}^{\epsilon} dx \Psi_{H1+}(x, y) + \Delta_0 e^{i\phi} \int_0^{\epsilon} dx \Psi_{E1-}^*(x, y) = E \int_{-\epsilon}^{\epsilon} dx \Psi_{E1+}(x, y), \quad (12)$$

Taking into account that the spinor $\Psi(x, y) = (\Psi_{E1+}(x, y), \Psi_{H1+}(x, y), \Psi_{E1-}^*(x, y), \Psi_{H1-}^*(x, y))$ is bounded in the region $[-\epsilon; \epsilon]$, the limit $\epsilon \rightarrow 0$ yields the relation

$$\lim_{\epsilon \rightarrow 0} (D + B) [\partial_x \Psi_{E1+}(\epsilon, y) - \partial_x \Psi_{E1+}(-\epsilon, y)] - \lim_{\epsilon \rightarrow 0} iA [\Psi_{H1+}(\epsilon, y) - \Psi_{H1+}(-\epsilon, y)] = 0. \quad (13)$$

The second term of the left-hand side is equal to zero, according to the continuity of the wavefunctions (otherwise the first order derivative are not defined). Hence $\partial_x \Psi_{E1+}(x, y)$ is also continuous at $x = 0$.

Following the same procedure for the three others differential equations, we obtain the complete set of boundary conditions

$$\begin{aligned}\Psi(x, y)|_{x \rightarrow 0^-} &= \Psi(x, y)|_{x \rightarrow 0^+} \\ \partial_x \Psi(x, y)|_{x \rightarrow 0^-} &= \partial_x \Psi(x, y)|_{x \rightarrow 0^+}.\end{aligned}\quad (14)$$

B. Average currents

We give here the derivation of the average current. The current operator in the x -direction is defined by¹⁵

$$J_x = \frac{\partial H}{\partial k_x} = \begin{pmatrix} -2D_+ k_x & A & 0 & 0 \\ A & -2D_- k_x & 0 & 0 \\ 0 & 0 & 2D_+ k_x & -A \\ 0 & 0 & -A & 2D_- k_x \end{pmatrix}, \quad (15)$$

where H is the Bogoliubov-de Gennes Hamiltonian appearing in Eq.(2) and with $D_{\pm} = D \pm B$. The average current for spin-up electrons writes

$$j_e(E) = \Psi_e^*(x) J_x \Psi_e(x), \quad (16)$$

where $\Psi_e(x)$ is defined in Eq.(4). Substituting Eqs.(4,15) into Eq.(16) leads to the expression Eq.(10) of the average current.

The average current for a reflected hole can be obtained by following the same procedure under the substitutions $\Psi_e(x) \rightarrow \Psi_h(x)$ and $k_{ex} \rightarrow k_{hx}$. Then the average current of reflected holes is

$$\begin{aligned}j_h(E, \theta) &= \mp 2k_1(-E) \cos \theta \{ D_+(d(\mathbf{k}) + M(\mathbf{k}))^2 \\ &\quad + A^2 k^2 D_- - A^2(d(\mathbf{k}) + M(\mathbf{k})) \},\end{aligned}\quad (17)$$

where the \mp sign refers to the conduction/valence band.

-
- ¹ X-L. Qi and S-C Zhang, *Physics Today* **63**, 33 (2010).
² J.E. Moore, *Nature* **464**, 194 (2010).
³ M.Z. Hasan and C.L. Kane, arXiv:1002.3895, 2010.
⁴ C.L. Kane and E.J. Mele, *Phys. Rev. Lett.* **95**, 226801 (2005).
⁵ B. A. Bernevig, T. L. Hughes, and S.C. Zhang. *Science* **314**, 1757 (2006).
⁶ L. Fu and C.L. Kane, *Phys. Rev. B* **76**, 045302 (2007).
⁷ H. Zhang et al., *Nature Physics* **5**, 438 (2009).
⁸ M. König, S. Wiedmann, C. Brüne, A. Roth, H. Buhmann, L. Molenkamp, X.-L. Qi, and S.C. Zhang, *Science* **318**, 766 (2007).
⁹ A. Roth, C. Bruene, H. Buhmann, L.W. Molenkamp, J. Maciejko, X-L Qi, S-C. Zhang, *Science* **325**, 294 (2009).
¹⁰ D. Hsieh et al., *Nature* **452**, 970 (2008).
¹¹ Y. Xia et al., *Nature Physics* **5**, 398 (2009).
¹² Y.L. Chen et al., *Science* **325**, 178 (2009).
¹³ Bin Zhou, H-Z. Lu, R-L. Chu, S-Q. Shen, and Q. Niu, *Phys. Rev. Lett.* **101**, 246807(2008).
¹⁴ T. Yokoyama, Y. Tanaka, and N. Nagaosa, *Phys. Rev. Lett.* **102**, 166801 (2009).
¹⁵ L.B. Zhang, K. Chang, X.C. Xie, H. Buhmann, and L.W. Molenkamp, arXiv:0912.3327, 2009.
¹⁶ E.G. Novik, P. Recher, E.M. Hankiewicz, and B. Trauzettel, *Phys. Rev. B* **81**, 241303 (2010).
¹⁷ X.-L. Qi, T. L. Hughes, S. Raghu, and S.-C. Zhang, *Phys. Rev. Lett.* **102**, 187001 (2009).
¹⁸ P. Hosur, S. Ryu, and A. Vishwanath, *Phys. Rev. B* **81**, 045120 (2010).
¹⁹ L. Fu and C. L. Kane, *Phys. Rev. Lett.* **100**, 096407 (2008).
²⁰ J. Nilsson, A.R. Akhmerov, and C.W.J. Beenakker, *Phys. Rev. Lett.* **101**, 120403 (2008).
²¹ A.R. Akhmerov, J. Nilsson, and C.W.J. Beenakker, *Phys. Rev. Lett.* **102**, 216404 (2009).
²² L. Fu and C. L. Kane, *Phys. Rev. Lett.* **102**, 216403 (2009).
²³ K. T. Law, P. A. Lee, and T. K. Ng, *Phys. Rev. Lett.* **103**, 237001 (2009).
²⁴ J. Linder, Y. Tanaka, T. Yokoyama, A. Sudbo, and N. Nagaosa, *Phys. Rev. Lett.* **104**, 067001 (2010).
²⁵ C. Nayak, S.H. Simon, A. Stern, M. Freedman, and S. Das Sarma, *Rev. Mod. Phys.* **80**, 1083 (2008).
²⁶ P. Adroguer, C. Grenier, D. Carpentier, J. Cayssol, P. Degiovanni and E. Orignac, *Phys. Rev. B* **82**, 081303(R) (2010).
²⁷ Y. S. Hor, A. J. Williams, J. G. Checkelsky, P. Roushan, J. Seo, Q. Xu, H. W. Zandbergen, A. Yazdani, N. P. Ong, and R. J. Cava, *Phys. Rev. Lett.* **104**, 057001 (2010).
²⁸ S. Chadov et al., arXiv:1003.0193, 2010.
²⁹ B. Yan et al., arXiv:1003.0074, 2010.
³⁰ A.F. Andreev, *Sov. Phys. JETP* **19**, 1228 (1964).
³¹ G.E. Blonder, M. Tinkham and T.M. Klapwijk, *Phys. Rev. B* **25**, 4515 (1982).
³² C.W.J. Beenakker, *Phys. Rev. Lett.* **97**, 067007 (2006).
³³ C.W.J. Beenakker, *Rev. Mod. Phys.* **80**, 1337 (2008).
³⁴ S. Bhattacharjee and K. Sengupta, *Phys. Rev. Lett.* **97**, 217001 (2006); J. Linder and A. Sudbo, *Phys. Rev. Lett.* **99**, 147001 (2007); J. Cayssol, *Phys. Rev. Lett.* **100**, 147001 (2008).
³⁵ C.X. Liu, T.L. Hughes, X-L. Qi, K. Wang, and S-C. Zhang, *Phys. Rev. Lett.* **100**, 236601 (2008); C-X. Liu, H. Zhang, B. Yan, X-L. Qi, T. Frauenheim, X. Dai, Z. Fang, and S-C. Zhang, *Phys. Rev. B* **81**, 041307(R) (2010); H-Z. Lu, W-Y. Shan, W. Yao, Q. Niu, S-Q. Shen, arXiv:0908.3120, 2009.
³⁶ T. Yokoyama, Y. Tanaka, and J. Inoue, *Phys. Rev. B* **74**, 035318 (2006).
³⁷ E. G. Novik, A. Pfeuffer-Jeschke, T. Jungwirth, V. Latussek, C. R. Becker, G. Landwehr, H. Buhmann, and L. W. Molenkamp, *Phys. Rev. B* **72**, 035321 (2005).
³⁸ M.I. Katsnelson, K.S. Novoselov, and A.K. Geim, *Nature Phys.* **2**, 620 (2006); Vadim V. Cheianov and Vladimir I. Falko, *Phys. Rev. B* **74**, 041403 (2006); J. Cayssol, B. Huard, and D. Goldhaber-Gordon, *Phys. Rev. B* **79**, 075428 (2009).